A Robust Adaptive Inverse Hyperbolic Sine Function (RA-IHSF)-based Controlled Solar PV Grid Integrated System

Shahzad Ali Rana[1] · **Majid Jamil**[1] · **Mumtaz Ahmad Khan**[2]

Abstract

This paper aims to maintain power quality for a two-stage solar photovoltaic (SPV) gird integrated system in case of dynamic disturbances such as unbalanced nonlinear load and variable solar irradiance. The proposed robust adaptive inverse hyperbolic sine function (RA-IHSF)-based control primarily extracts the fundamental load current weight component and is employed to control the voltage source converter (VSC) by altering the switching patterns of pulses. The maximum power can be retrieved from the SPV generation system by implementing a maximum power point tracking control based on incremental conductance method along with DC-to-DC boost converter. The VSC feeds active power to load and grid together with reactive power compensation. The proposed control technique also provides load balancing and mitigates harmonic content of grid current along with power factor correction. The response of the system to the implementation of proposed RA-IHSF illustrates that it is more expedient as compared to conventional adaptive filter-based algorithms showing improved dynamic response with less computational burden.

Keywords Two-staged solar photovoltaic (SPV) system · Robust adaptive inverse hyperbolic sine function (RA-IHSF) · Incremental conductance (INC) · Voltage source controller (VSC) · Nonlinear load and solar irradiance

1 Introduction

Recent data suggest the growing importance of renewable energy sources compared to conventional energy sources throughout the world. The degree of penetration of renewable resources in the electric utility grid has also increased substantially in the last decade as policies to incentivize and promote their development are enacted. Among the renewable sources, solar photovoltaic seems to be an appealing energy solution. It provides a wide variety of end-use applications, from commercial utilities to residential rooftops. When effectively harnessed, energy from SPVs has the potential to meet all of the world's current and projected needs [1–5]. Because of all of its benefits, SPVs are expected to become an essential renewable source during the energy transition to sustainable development in the twenty-first century. Various attempts in the form of improved control strategies have been reported to better integrate SPV generation with the electric utility grid. According to their application, SPV systems may exist in on-grid/off-grid single-stage/double-stage configurations [6]. From the review of various published scientific articles, it can be observed that there are primarily two control objectives that are identified for any of the control algorithms described for the integration of SPV systems: the first being MPPT control and the second being power electronics converter (VSC) control [7–14].

The aim of the MPPT control is to extract the maximum amount of power from SPV array under all situations so that the operational efficiency of the SPV system is improved. Therefore, the selection of a suitable MPPT control is essential. Various MPPT techniques for SPV systems have been discussed and compared in [15]. The traditional perturb and observe (P & O) MPPT technique operates by perturbing the SPV array voltage by a set value and then monitoring the change in power [16]. It is simple to implement but suffers

✉ Shahzad Ali Rana
shahzad.alirana1988@gmail.com

Majid Jamil
mjamil@jmi.ac.in

Mumtaz Ahmad Khan
makhan2@jmi.ac.in

1 Department of Electrical Engineering, Jamia Millia Islamia, New Delhi, India

2 Electrical Engineering Section, Jamia Millia Islamia, New Delhi, India

the drawback of occasional deviations from the MPPT under rapidly changing irradiance levels. The implementation of the INC-based algorithm [17] is comparable in complexity to the P and O technique but offers a higher yield under varying levels of irradiance. Several intelligent techniques based on fuzzy control, neural network control and particle swarm optimization have been presented throughout [18–22]. These operate well under the conditions of partial shading and varying atmospheric conditions. The MPPTs based on intelligent techniques do not require an accurate model of the SPV array but may require retuning from time to time.

The type of the load(s) connected at the PCC will determine the amount of reactive power and harmonic drawn from the grid in the absence of any other sources at the PCC. The extensive use of nonlinear loads and occurrence of dynamic disturbances such as unbalanced nonlinear load and variable solar irradiance at PCC lead to various power quality problems reported in [23, 24]. However, the proper operation of the VSC connected at PCC may serve to offer ancillary functions such as harmonics reduction, load balancing, injection of reactive power and hence power factor correction at the point of common coupling (PCC). Thus, there is a need to continually improve VSC control algorithms to achieve [25–28] flexible and reliable interfacing of SPV systems with the electric utility grid. Different conventional and adaptive control schemes for VSC control have been presented in the literature. Synchronous reference frame theory (SRFT) or d–q control is one of the conventional schemes based on indirect current control technique that employs coordinate transformations (Clarke transformation to convert abc to $\alpha\beta$ and Park transformation to convert $\alpha\beta$ to dq) to generate DC components of measured parameters for the purpose of VSC control. The control technique maintains the voltage at the PCC along with power factor correction. The SRFT or d–q algorithm when employed with low-pass filter to estimate the direct axis component results in elimination of harmonic components but also degrades the power quality in the distribution grid [29]. Also, SRFT or d–q theory-based control scheme needs to be implemented with PLL (phase-locked loop) to generate unit voltage templates (sine and cosine signals) which results in more computational burden. The instantaneous reactive power theory (IRPT) or p–q-based control algorithm accuracy is largely synchronous frame accuracy dependent. It is based on Clarke transformation to convert rotating frame DC variables into stationary frame AC variables. Then, these components are used to calculate the three-phase active and reactive power. The second harmonic component is mitigated from the estimated powers by employing LPF which makes the system transient response sluggish [30–32]. The second-order generalized integrator (SOGI) shows improvement in steady-state performance along with fast dynamic response [33]. However, it is failed to track fundamental load

current accurately whenever there is a change in frequency. Hyperbolic tangent function-based least mean square (LMS) control has a very fast dynamic response, but it suffers from large oscillations [34] The adaptive filter theory [35]-based LMS, least mean fourth (LMF), sign-error and normalized LMS control have shown their potential in tracking in varying atmospheric conditions and characteristics. However, while computing weight component corresponding to load current, large steady-state oscillations are associated with LMS and the LMF suffers with slow convergence speed [36–38]. A new control algorithm is introduced in [39] obtained by modifying least mean fourth (LMF) so as power quality of SPV system interfaced with distribution grid is improved. Because of fourth-order optimization, the scheme shows good performance in dynamic conditions. However, the scheme is subjected to some shortcomings such as poor steady-state performance and non-capability of DC offset elimination.

The major concern of the proposed work is to maintain power quality for a two-stage SPV gird integrated system in case of dynamic disturbances. The reference grid currents can be obtained by implementation of proposed RA-IHSF algorithm [40] whose main object is extraction of fundamental load current weight components. A robust adaptive technique employing the inverse hyperbolic sine function can provide better steady-state performance and stronger robustness as compared to conventional adaptive filtering algorithms. The performance of the system to implementation of proposed RA-IHSF illustrates that it is more expedient as compared to conventional adaptive filters (for example, LMS and LMF)-based algorithms showing improved dynamic response with less computational burden. Thus, the main aspects of the proposed work are as follows:

- Utilization of SPV power to feed load.
- Sinusoidal and balanced grid current in dynamic disturbances such as unbalancing of load and varying solar insolation.
- Reactive power compensation to load from VSC instead of grid.
- Power factor correction (PFC) operation.

2 System Description

A three-phase, 415 V, 50 Hz grid integrated with a two-stage 44 kW SPV system along with a nonlinear load connected at the PCC is shown in Fig. 1. A DC-link capacitor is required so that SPV array can be interfaced with VSC. The SPV system is incorporated with a DC-to-DC boost converter, and an incremental conductance-based MPPT technique is executed to extract maximum SPV power from the SPV modules. An interfacing inductor is added to the system so as to reduce
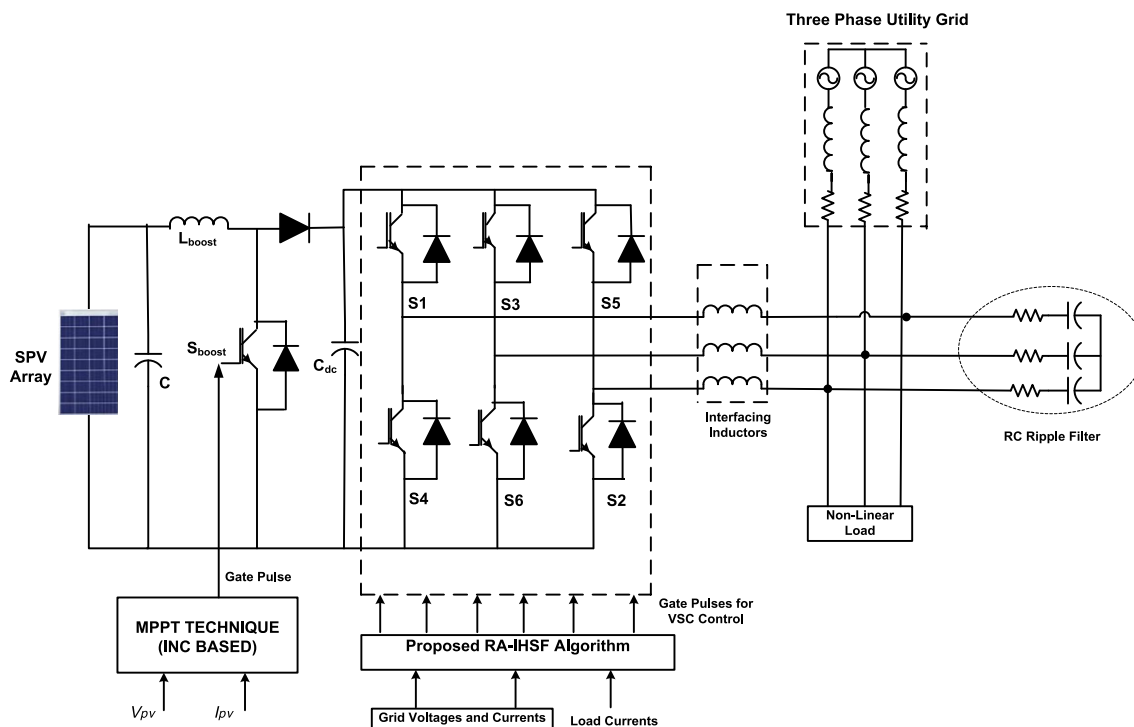
Fig. 1 Proposed system topology

the ripple in VSC current. The pulses of controlled switching patterns in VSC are generated by the application of proposed RA-IHSF algorithm [40] in grid integrated SPV system. The various components in proposed configuration are estimated in this section.

The voltage magnitude of DC link ($V_{\text{dc−link}}$) is obtained by the following relation:

$$V_{\text{dc−link}} = 2\sqrt{2}V_{ll} \Big/ \sqrt{3}m_i \tag{1}$$

where V_{ll} is line-to-line voltage and m_i is the modulation index.

The SPV modules need to be in a single series string (N_S) is obtained as

$$N_s = V_{\text{dc\_link}}/V_{\text{mpp}} \tag{2}$$

where V_{mpp} is rated voltage of SPV array at 1000 W/m^2 and 25 °C.

Similarly, the number of series strings connected in parallel (N_P) is estimated as

$$N_P = \left(P_{\text{max}}/V_{\text{dc\_link}}\right)/I_{\text{mpp}} \tag{3}$$

where P_{max} and I_{mpp} is rated power and current of SPV array at 1000 W/m^2 and 25 °C, respectively.

The inductor present in DC–DC boost converter is calculated using Eq. (4) [24]

$$L_{\text{boost}} = V_{\text{mpp}} \cdot \text{Duty\_}Cycle \Big/ \Delta I_a \cdot f_{\text{sw}} \tag{4}$$

The value of duty cycle can be obtained from MPPT, whereas ΔI_a is the amount of array current's ripple, while f_{sw} is boost converter switching frequency. The value of interfacing inductor for reducing ripple in VSC current can be calculated using (5) [24]

$$L_{\text{if}} = \sqrt{3} \cdot m \cdot V_{\text{dc - link}} \Big/ 12 \cdot \lambda \cdot f_{\text{vsc}} \cdot \Delta I_{\text{rip}} \tag{5}$$

where m is modulation index, λ is overloading factor, f_{vsc} is switching frequency, and the rated ripple current is denoted by ΔI_{rip}. Here, the value of interfacing inductor is chosen as 2.5 mH. The value of capacitance and resistance of RC filter is set to be 10^{-5} F and 5 Ω. The capacitance (C_{dc}) associated with DC link is obtained using (6) [24]

$$C_{\text{dc}} = P_{\text{dc}} \Big/ 2 \cdot \omega \cdot V_{\text{dc - link}} \cdot V_{\text{dcr}} \tag{6}$$

The parameters of various components shown in Fig. 1 are estimated and tabulated in Table 1.

Ⓛ ☺ Springer

Table 1 Proposed system parameters

Parameters	Values
Rating of SPV array	44 kW
Open-circuit voltage/module (V_{OC})	33.53 V
Short-circuit current/module (I_{SC})	8.24 A
Rated power/module at 1000W/m^2 and 25 °C (P_{max})	200.24 W
Rated voltage of SPV array at 1000W/m^2 and 25 °C ((V_{mpp}))	558.4 V
Rated current od SPV array at 1000W/m^2 and 25 °C (I_{mpp})	78.9 A
SPV modules need to be in a single series string (N_S)	22
Number of series strings connected in parallel (N_P)	10
Boost inductor (L_{boost})	3 mH
VSC-DC-link voltage ($V_{dc\text{-}link}$)	700 V
DC-link capacitance (C_{dc})	6000 μF
Interfacing inductor (L_{if})	2.5 mH
Ripple filter parameters	$R = 5\ \Omega$ and $C = 10\ \mu F$
Utility grid	Three-phase, 415 V, 50 Hz
Nonlinear load	3-phase diode rectified series RL load of 25 Ω and 150 mH

3 Control Algorithm

The proposed work is carried out based on two-stage topology of power conversion for integration of SPV with three-phase system. The proposed control scheme is designed to extract maximum SPV power and to maintain power quality at PCC while feeding the extracted solar power to connected loads and grid. Therefore, the overall control consists of two main approaches, namely MPPT control for maximum power extraction and the grid-connected VSC control.

3.1 Control for MPPT

The maximum power can be retrieved from the SPV generation system by implementing a DC-to-DC boost converter with INC-based MPPT control. In INC-based MPPT, the slope of P–V characteristics of SPV system is varied in accordance to the ratio of incremental conductance to instantaneous conductance. Thus, duty cycle of converter is altered as per variation in slope [14].

3.2 Control for Grid-Connected VSC

The grid-connected VSC is operated on the basis of pattern of switching pulses for IGBT-based power electronics switches configured to form VSC as shown in Fig. 2. The proposed control method utilizes a hysteresis current controller (HCC) to produce gating pulses by comparing reference and sensed grid currents. The reference grid currents are estimated by evaluating different weight components. Therefore, the proposed work is about the estimation of active weight component, ψ_{sp}, which includes weight component based upon amount of SPV generated power ψ_{pv}, weight component corresponding to value of DC-link voltage, ψ_{dc}, and active weight component corresponding to load current ψ_{lp}. The reactive component, ψ_{sq}, comprises weight component corresponding to terminal voltage at PCC, ψ_{tq}, and weight component based on reactive component of load current, ψ_{lq}.

3.2.1 Robust Adaptive Inverse Hyperbolic Sine Function (RA-IHSF) Algorithm

A robust adaptive technique employing the inverse hyperbolic sine function (IHSF) provides better steady-state performance and stronger robustness when compared to other adaptive filtering algorithms [40].

The cost function of the proposed algorithm is given by:

$$L(\theta) = \arg\min J[L(\theta)]$$
$$= \arg\min\left[\sinh^{-1}\left(e^2(\theta)\right)\right] \tag{7}$$

where $e(\theta)$ is estimated error signal of the proposed algorithm.

The calculation of estimated error signal in proposed algorithm is carried out by equation,

$$e(\theta) = \mathrm{d}(\theta) - \psi^T(\theta) \cdot x(\theta) \tag{8}$$

where $x(\theta)$ is input vector. In the modelling of RA-IHSF control for VSC, these vectors are termed as unit in-phase vectors (x_{pa}, x_{pb}, x_{pc}) and unit quadrature vectors (x_{qa}, x_{qb}, x_{qc}), which are required to generate reference active and reactive grid currents. The response $\mathrm{d}(\theta)$ is modelled as, $\mathrm{d}(\theta) = \psi_0^T(\theta) \times x(\theta) + v(\theta)$, where ψ_0 represents the optimal weight vector, while $v(\theta)$ represents the source of noise. For given input $x(\theta)$ and weight value $\psi(\theta)$, the estimated output is represented by term $\psi^T(\theta) \cdot x(\theta)$.

The gradient term for the optimization of algorithm is obtained as:

$$= \frac{\partial J(\psi(\theta))}{\partial \psi(\theta)} = \frac{\partial\left(\sinh^{-1}\left(e^2(\theta)\right)\right)}{\partial \psi(\theta)} = \frac{-2}{\sqrt{1+e^2(\theta)}}e(\theta) \cdot x(\theta) \tag{9}$$
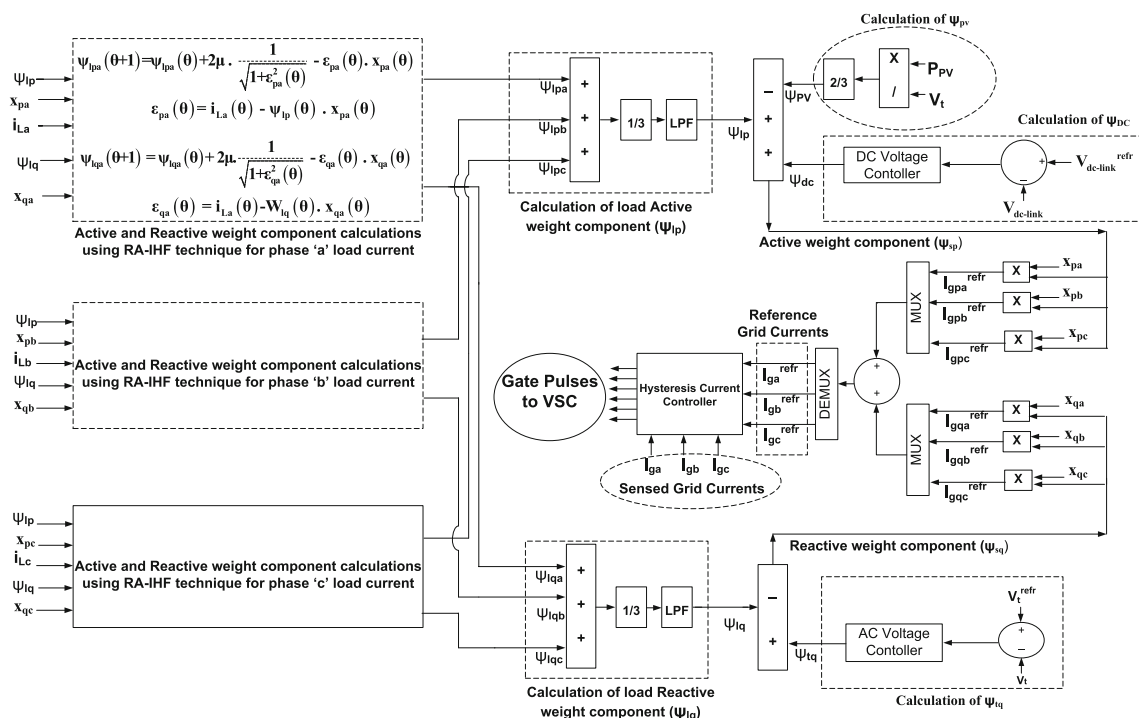
Fig. 2 Proposed control algorithm

The iterative scheme is given by:

$$\psi(\theta + 1) = \psi(\theta) - \mu \frac{\partial J(\psi(\theta))}{\partial \psi(\theta)} \tag{10}$$

$$\psi(\theta + 1) = \psi(\theta) + \frac{2\mu}{\sqrt{1 + e^2(\theta)}} e(\theta) \cdot x(\theta) \tag{11}$$

where μ is the step size.

3.2.2 Generation of Reference Grid Currents

The generation of reference grid currents is subdivided into several stages as per the sequence of operations.

Estimation of Unit Templates The line-to-neutral voltages (v_{ga}, v_{gb}, v_{gc}) are estimated at PCC using (12) [24]

$$\begin{bmatrix} v_{ga} \\ v_{gb} \\ v_{gc} \end{bmatrix} = \frac{1}{3} \begin{bmatrix} 2 & 1 \\ -1 & 1 \\ -1 & 2 \end{bmatrix} \begin{bmatrix} v_{gab} \\ v_{gbc} \end{bmatrix} \tag{12}$$

where v_{gab} and v_{gbc} are PCC line-to-line voltages.
The magnitude of terminal voltage (V_t) is estimated as:

$$V_t = \sqrt{0.66 \cdot \left(v_{ga}^2 + v_{gb}^2 + v_{gc}^2 \right)} \tag{13}$$

The in-phase unit templates (x_{pa}, x_{pb}, x_{pc}) are determined using (14)

$$\begin{bmatrix} x_{pa} \\ x_{pb} \\ x_{pc} \end{bmatrix} = \frac{1}{V_t} \begin{bmatrix} v_{ga} \\ v_{gb} \\ v_{gc} \end{bmatrix} \tag{14}$$

The unit templates in-quadrature $(x_{qa}, x_{qb}$ and $x_{qc})$ can be derived using (15)

$$x_{qa} = \frac{-x_{pb} + x_{pc}}{\sqrt{3}},$$
$$x_{qb} = \frac{\sqrt{3} x_{pa}}{2} + \frac{(x_{pb} - x_{pc})}{2\sqrt{3}},$$
$$x_{qc} = -\frac{\sqrt{3} x_{pa}}{2} + \frac{(x_{pb} - x_{pc})}{2\sqrt{3}} \tag{15}$$

Estimation of Weight Component Corresponding to DC-Link Voltage (ψ_{dc}) and Terminal Voltage at PCC (ψ_{tq}) The weight component, ψ_{dc}, for sustaining DC-link voltage at VSC side is determined using (16) and (17)

$$V_{dc\text{-}link}^{err}(\theta) = V_{dc\text{-}link}^{refr}(\theta) - V_{dc\text{-}link}(\theta) \tag{16}$$

where $V_{dc\text{-}link}^{err}$ is the deviation of reference DC-link voltage ($V_{dc\text{-}link}^{ref}$) from actual DC-link voltage ($V_{dc\text{-}link}$) at VSC. $V_{dc\text{-}link}^{err}$ is utilized for obtaining weight component

ψ_{dc} in PI controller which can be estimated as,

$$
\begin{aligned}
\psi_{dc}(\theta + 1) = \psi_{dc}(\theta) &+ \xi_i V_{dc\text{-link}}^{err}(\theta + 1) \\
&+ \xi_p \{ V_{dc\text{-link}}^{err}(\theta + 1) - V_{dc\text{-link}}^{err}(\theta) \}
\end{aligned} \tag{17}
$$

where ξ_i and ξ_p represent the integral gain and proportional gain, respectively, for the PI controller.

Likewise, another PI controller regulates the magnitude of PCC voltage (V_t) so that it tracks the PCC voltage reference (V_t^{refr}). The PCC voltage error is given by

$$
V_t^{err}(\theta) = V_t^{refr}(\theta) - V_t(\theta) \tag{18}
$$

where V_t^{err} is utilized for obtaining quadrature phase loss component ψ_{tq} in PI controller which is used to regulate the PCC voltage and can be estimated as,

$$
\begin{aligned}
\psi_{tq}(\theta + 1) = \psi_{tq}(\theta) &+ \xi_i V_t^{err}(\theta + 1) \\
&+ \xi_p \{ V_t^{err}(\theta + 1) - V_t^{err}(\theta) \}
\end{aligned} \tag{19}
$$

SPV Feed-Forward Component (ψ_{pv}) SPV feed-forward component (ψ_{pv}) corresponding to extracted SPV power can be estimated as:

$$
\psi_{pv}(\theta) = 2 \cdot P_{PV}(\theta) / 3 \cdot V_t \tag{20}
$$

where P_{PV} is maximum extracted SPV power with the aid of MPPT technique.

Active and Reactive Weight Components Corresponding to Load Current The value of the active weight component corresponding to load current can be found out with the proposed RA-IHSF algorithm. The weight ψ_{lpa} corresponding to phase 'A' load current, i_{La}, is estimated as:

$$
\begin{aligned}
\psi_{lpa}(\theta + 1) = \psi_{lpa}(\theta) &+ 2\mu \cdot \frac{1}{\sqrt{1 + \varepsilon_{pa}^2(\theta)}} \\
&- \varepsilon_{pa}(\theta) \cdot x_{pa}(\theta)
\end{aligned} \tag{21}
$$

where μ is step size.

The error $\varepsilon_{pa}(\theta)$ is defined using (22).

$$
\varepsilon_{pa}(\theta) = i_{La}(\theta) - \psi_{lp}(\theta) \cdot x_{pa}(\theta) \tag{22}
$$

Likewise, the active weight components concerned to load currents of phase 'B' and 'C' are obtained using (23) and (25).

$$
\begin{aligned}
\psi_{lpb}(\theta + 1) = \psi_{lpb}(\theta) &+ 2\mu \cdot \frac{1}{\sqrt{1 + \varepsilon_{pb}^2(\theta)}} \\
&- \varepsilon_{pb}(\theta) \cdot x_{pb}(\theta)
\end{aligned} \tag{23}
$$

where

$$
\varepsilon_{pb}(\theta) = i_{Lb}(\theta) - \psi_{lp}(\theta) \cdot x_{pb}(\theta) \tag{24}
$$

$$
\begin{aligned}
\psi_{lpc}(\theta + 1) = \psi_{lpc}(\theta) &+ 2\mu \cdot \frac{1}{\sqrt{1 + \varepsilon_{pc}^2(\theta)}} \\
&- \varepsilon_{pc}(\theta) \cdot x_{pc}(\theta)
\end{aligned} \tag{25}
$$

where

$$
\varepsilon_{pc}(\theta) = i_{Lc}(\theta) - \psi_{lp}(\theta) \cdot x_{pc}(\theta) \tag{26}
$$

Similarly, the value of reactive weight component of phase 'A' load current is determined as:

$$
\begin{aligned}
\psi_{lqa}(\theta + 1) = \psi_{lqa}(\theta) &+ 2\mu \cdot \frac{1}{\sqrt{1 + \varepsilon_{qa}^2(\theta)}} \\
&- \varepsilon_{qa}(\theta) \cdot x_{qa}(\theta)
\end{aligned} \tag{27}
$$

where μ is step size.

The error $\varepsilon_{qa}(\theta)$ is defined using (28)

$$
\varepsilon_{qa}(\theta) = i_{La}(\theta) - W_{lq}(\theta) \cdot x_{qa}(\theta) \tag{28}
$$

Likewise, the reactive weight components concerned to load currents of phase 'B' and 'C' are obtained using (29) and (31)

$$
\begin{aligned}
\psi_{lqb}(\theta + 1) = \psi_{lqb}(\theta) &+ 2\mu \cdot \frac{1}{\sqrt{1 + \varepsilon_{qb}^2(\theta)}} \\
&- \varepsilon_{qb}(\theta) \cdot x_{qb}(\theta)
\end{aligned} \tag{29}
$$

where

$$
\varepsilon_{qb}(\theta) = i_{Lb}(\theta) - W_{lq}(\theta) \cdot x_{qb}(\theta) \tag{30}
$$

$$
\psi_{lqc}(\theta + 1) = \psi_{lqc}(\theta) + 2\mu \cdot \frac{1}{\sqrt{1 + \varepsilon_{qc}^2}} - \varepsilon_{qc}(\theta) \cdot x_{qc}(\theta) \tag{31}
$$

where

$$
\varepsilon_{qc}(\theta) = i_{Lc}(\theta) - W_{lq}(\theta) \cdot x_{qc}(\theta) \tag{32}
$$

Calculation of Grid Reference Currents To calculate the total active grid reference current weight component (ψ_{sp}), a sign convention is used. The load and loss components which show power consumption at the PCC are assigned a positive sign, while the SPV feed-forward component which shows power input is assigned a negative sign. The total active grid reference current weight component (ψ_{sp}) is calculated by

algebraically summing the weight component corresponding to DC-link voltage (ψ_{dc}) to the average active load current component (ψ_{lp}) and subtracting the SPV feed-forward component (ψ_{pv}).

$$\psi_{sp} = \psi_{lp} + \psi_{dc} - \psi_{pv} \tag{33}$$

where

$$\psi_{lp} = \left(\psi_{lpa} + \psi_{lpb} + \psi_{lpc}\right)/3 \tag{34}$$

Similarly, the total reactive grid reference current component (ψ_{sq}) is calculated by subtracting the average reactive load current weight component (ψ_{lq}) from the weight component corresponding to terminal voltage at PCC (ψ_{tq}),

$$\psi_{sq} = \psi_{tq} - \psi_{lq} \tag{35}$$

where

$$\psi_{lq} = \left(\psi_{lqa} + \psi_{lqb} + \psi_{lqc}\right)/3 \tag{36}$$

The active reference grid currents are evaluated using (37)

$$\begin{bmatrix} i_{gpa}^{refr} \\ i_{gpb}^{refr} \\ i_{gpc}^{refr} \end{bmatrix} = \psi_{sp} \begin{bmatrix} x_{pa} \\ x_{pb} \\ x_{pc} \end{bmatrix} \tag{37}$$

Similarly, the reactive reference grid currents are evaluated as:

$$\begin{bmatrix} i_{gqa}^{refr} \\ i_{gqb}^{refr} \\ i_{gqc}^{refr} \end{bmatrix} = \psi_{sq} \begin{bmatrix} x_{qa} \\ x_{qb} \\ x_{qc} \end{bmatrix} \tag{38}$$

The total three-phase reference grid currents are calculated by summing up the active and reactive reference grid currents.

$$i_{ga}^{refr} = i_{gpa}^{refr} + i_{gqa}^{refr}, \; i_{gb}^{refr} = i_{gpb}^{refr} + i_{gqb}^{refr}, \; i_{gc}^{refr}$$
$$= i_{gpc}^{refr} + i_{gqc}^{refr} \tag{39}$$

The proposed control method with a hysteresis current controller (HCC) is utilized to produce gating pulses for switching of the VSC switching devices. The error signals are computed by comparing actual (i_{ga}, i_{gb}, i_{gc}) and reference grid currents (i_{ga}^{refr}, i_{gb}^{refr}, i_{gc}^{refr}). The error signals are then sent through the HCC which generates gating pulses.

4 Results and Discussion

The proposed two-stage SPV gird integrated system with nonlinear load is simulated using RA-IHSF, and the performance of the system is depicted in results. For nonlinear load, the results depict the solar power extraction and reactive power compensation while also providing load balancing at different dynamic conditions such as unbalanced nonlinear load and variable solar irradiance. To illustrate the performance, the waveform of solar irradiance (G), PCC voltages (v_g), grid currents (i_g), grid real power (P_G), grid reactive power (Q_G), DC-link voltage (V_{DC}), phase 'a' load current (i_{La}), load real power (P_L), VSC current (i_{inv}), VSC real power (P_C), SPV voltage (V_{PV}), SPV current (I_{PV}), SPV power (P_{PV}) and various calculated weights such as ψ_{lp}, ψ_{pv}, ψ_{dc} and ψ_{sp} are shown in Figs. 3, 4, 5 and 6 for different conditions. The THD analysis of load current, grid voltage and current is also shown in these figures.

4.1 Steady-State Behaviour of Proposed System

The suggested system steady-state performance is obtained by simulating it with a nonlinear load connected at the PCC, and the response is presented in Fig. 3. The phase voltages (v_g) and the phase currents (i_g) of grid are found to be sinusoidal. The phase angle is 180 degree between phase voltages and currents of grid for each phase indicating grid's unity power factor operation. The load current waveform for phase 'A' (i_{La}) and the VSC output current waveform for phase 'A' (i_{inv}) show their non-sinusoidal nature. Also, the PI controller is firmly maintained the voltage magnitude of VSC-DC link (V_{DC}) to 700 V. The SPV array operates at maximum power point (I_{PV} and V_{PV}) with INC MPPT and so generating maximum power (P_{PV}) at irradiance (G) of 1000 W/m^2. The grid active power output (P_G) is negative because the VSC is supplying a part of active power generated by the SPV array (P_{PV}) back to the grid after full filling the load active demand (P_L). As a result, the grid is absorbing power rather than delivering it. The grid reactive power output (Q_G) is zero as the VSC supplies the reactive power requirements of the load. The total active grid reference current component (ψ_{sp}), weight component corresponding to DC-link voltage (ψ_{dc}), the average active load component (ψ_{lp}) and SPV feed-forward component (ψ_{pv}) are also shown. Also, the total harmonic distortion value for the grid voltage and load current is 0.03% and 23.63%, respectively. The % THD in grid current is found to be 0.28% which is well in agreement with the 5% suggested by the IEEE-519 standard.
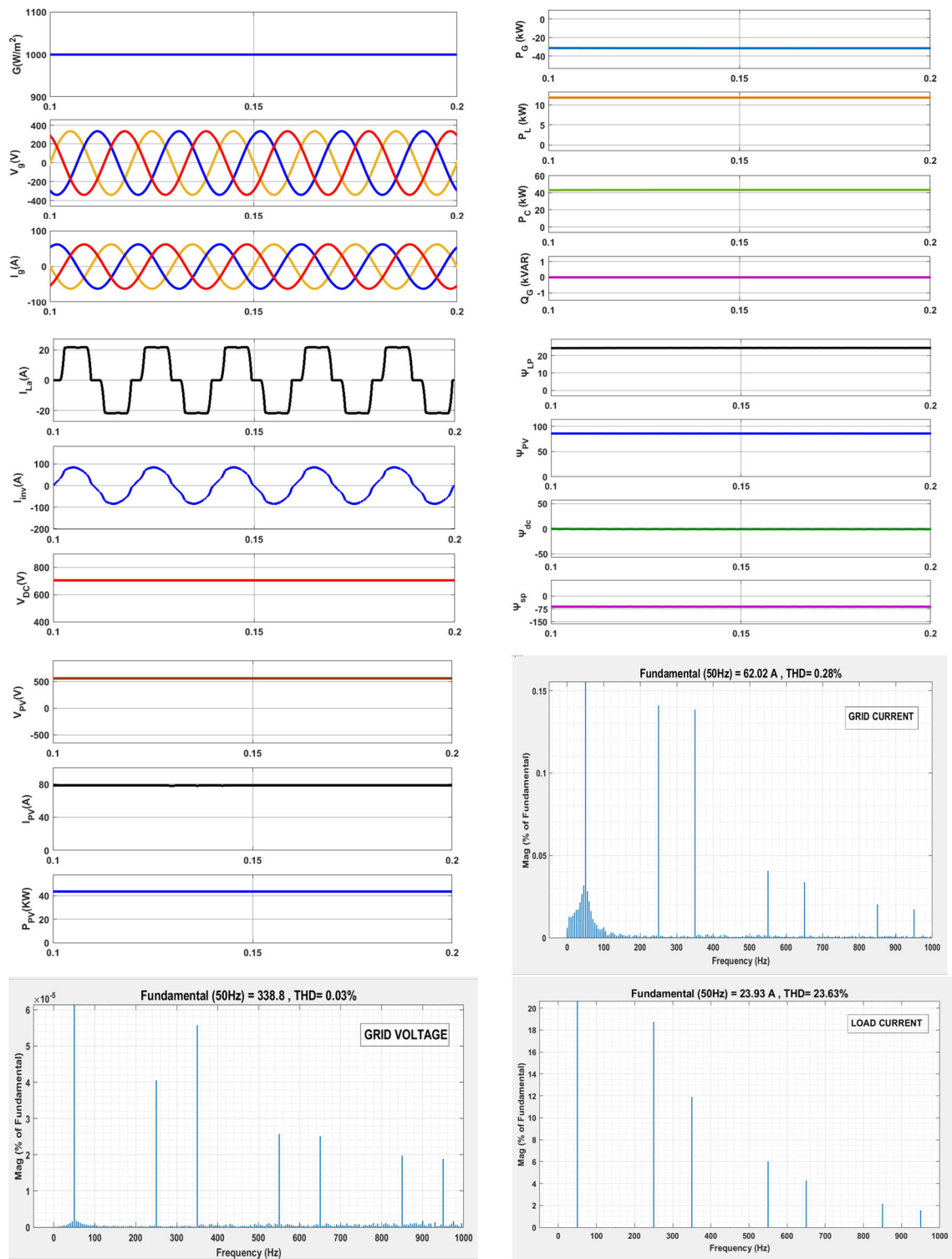
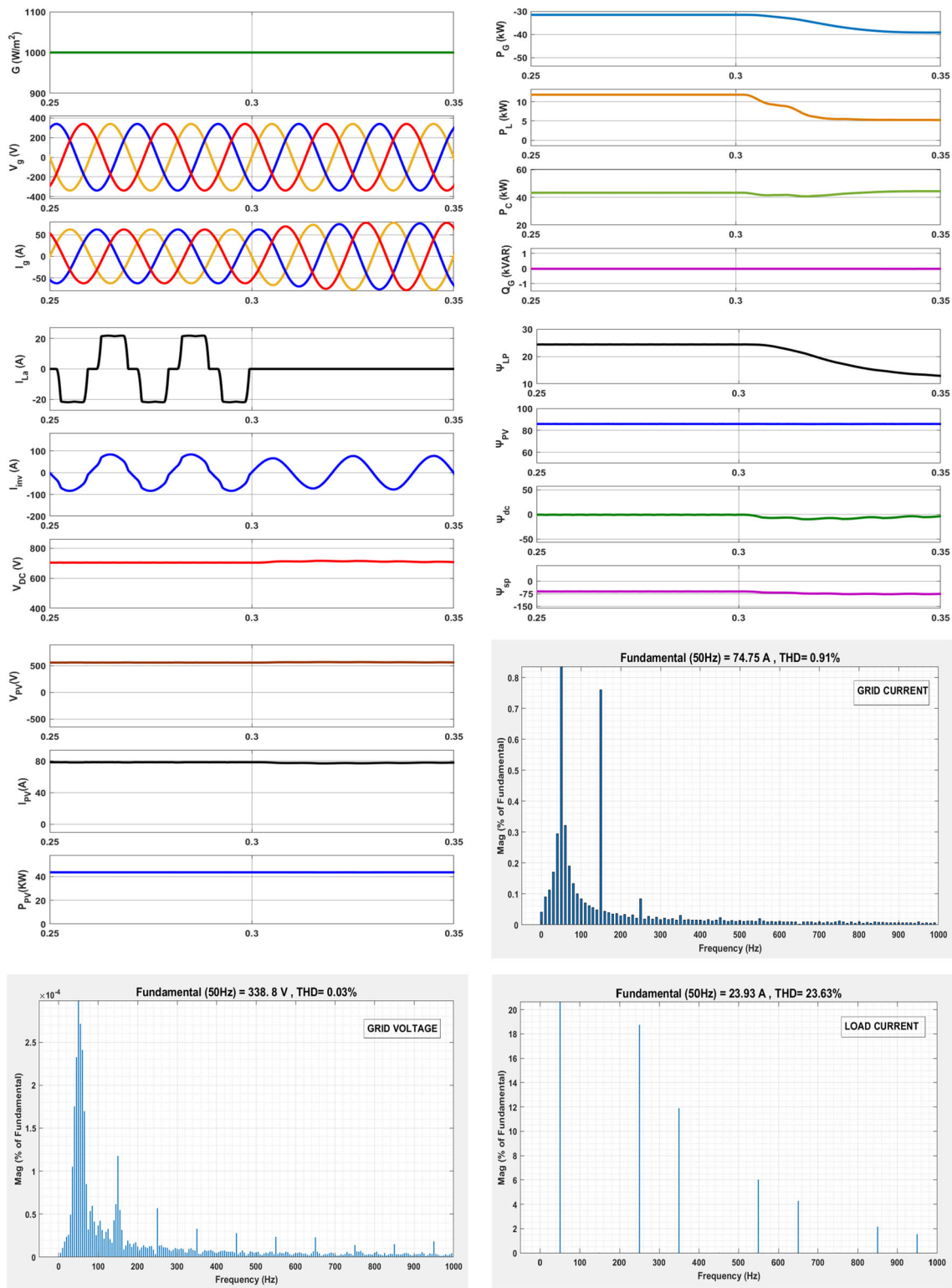**Fig. 3** Response for steady-state behaviour proposed system

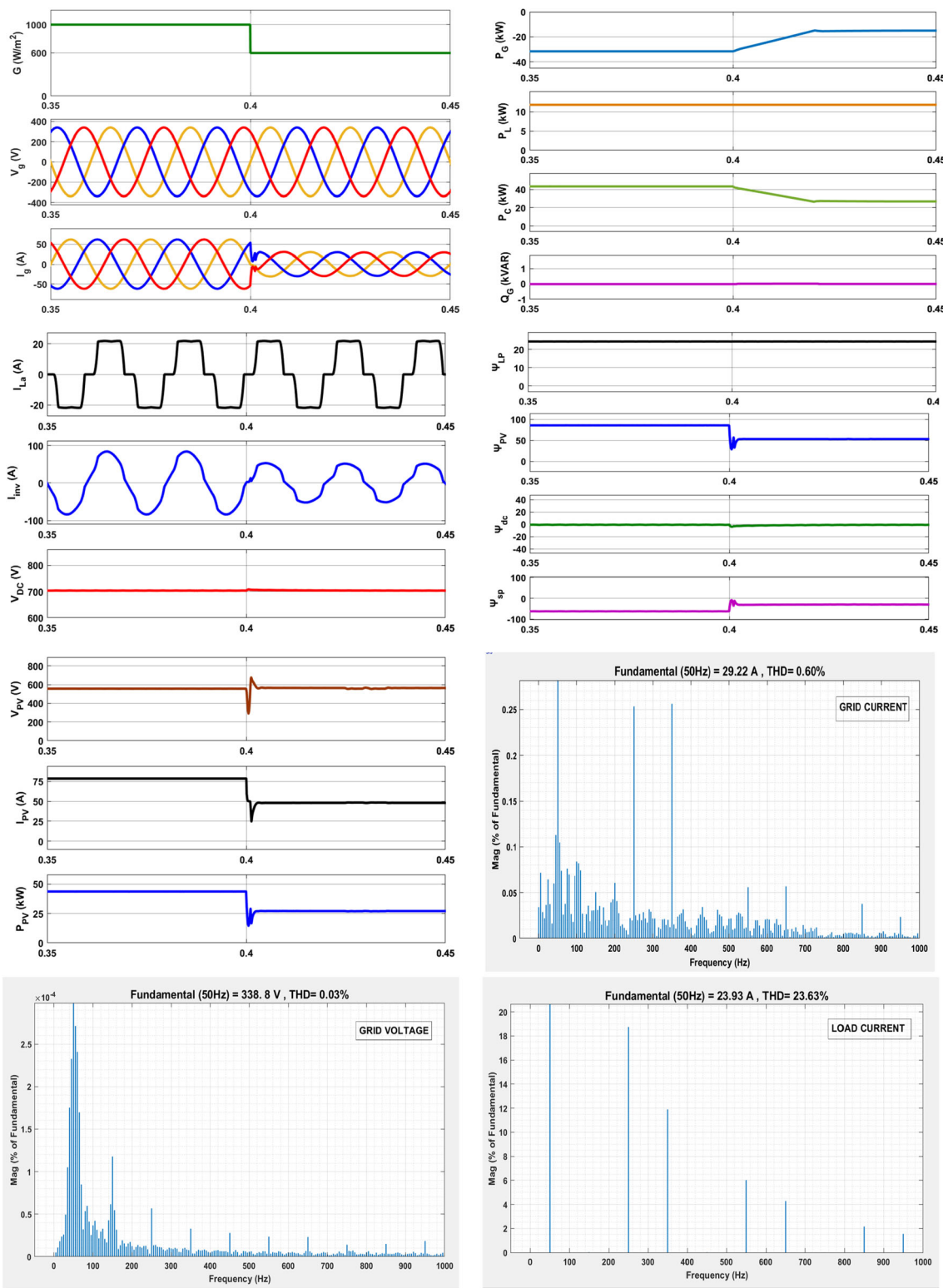**Fig. 4** System response for unbalancing of nonlinear load

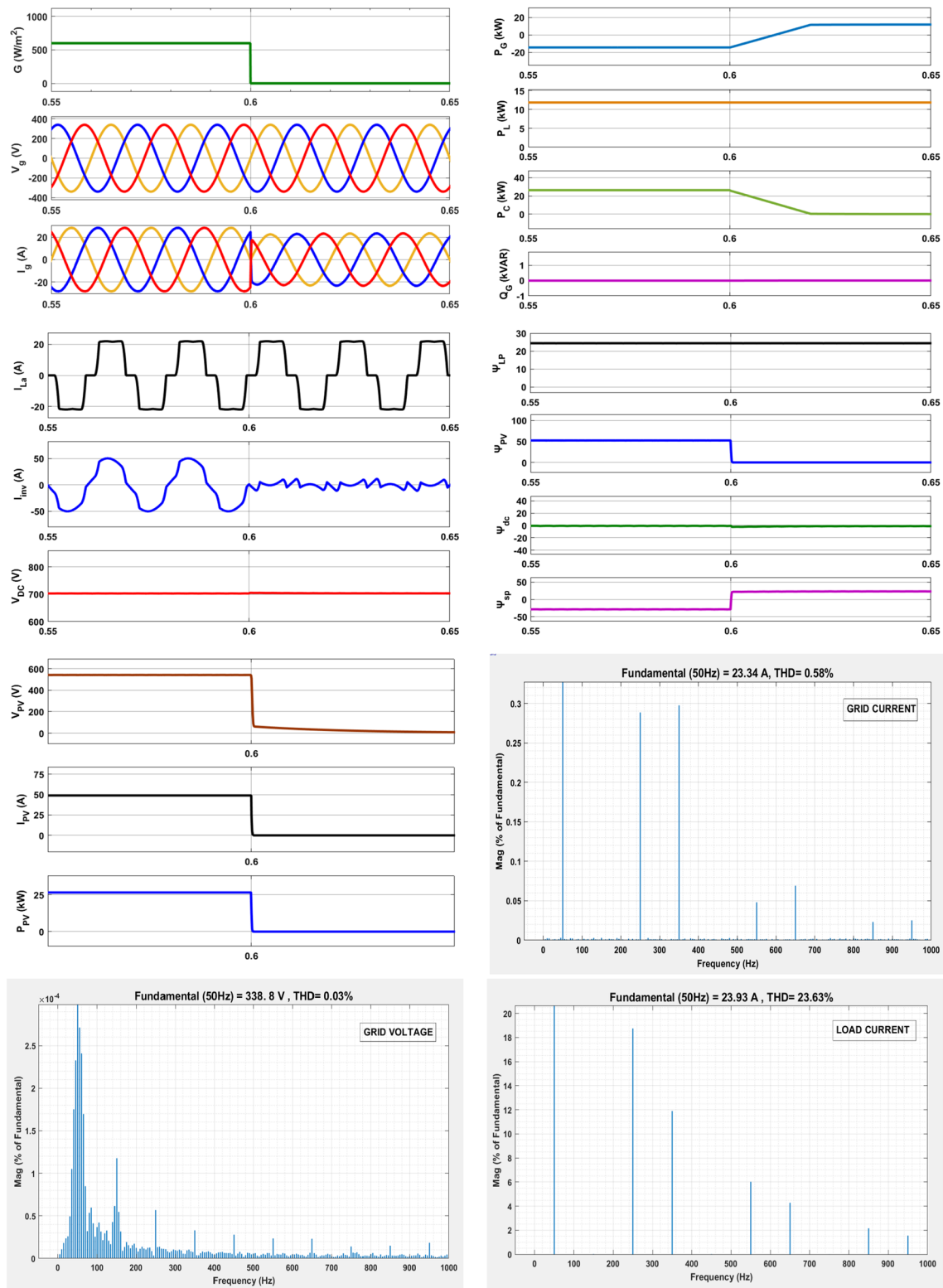**Fig. 5** Response of the system for varying irradiance

Fig. 6 System response for zero solar irradiance

4.2 Dynamic Behaviour Under Unbalanced Nonlinear Load

To simulate an unbalanced load, the load connected to phase 'A' is removed at 0.3 s and the behaviour of the system is observed and the response is presented in Fig. 4. The phase voltages (v_g) and the phase currents (i_g) of grid are found to be sinusoidal. Also, the phase angle between phase voltage and current of grid is 180 degree indicating grid's ability to sustained unity power factor operation during load unbalancing. After 0.3 s, grid current is increased which means more power is transferred to grid as load demand reduces due to phase removal. The load current waveform for phase 'A' (i_{La}) and the VSC output current waveform for phase 'A' (i_{inv}) show their non-sinusoidal nature. Also, results shows that the magnitude of phase 'A' becomes zero after phase removal at 0.3 s. The SPV array still operates at maximum power point (I_{PV} and V_{PV}) generating maximum power (P_{PV}) as there is no change in irradiance, and only load is unbalanced. The grid active power output (P_G) is negative because the VSC is supplying a part of active power from SPV array (P_{PV}) back to the grid after full filling the active load demand (P_L). However, the negative magnitude of P_G is increased after load unbalancing at 0.3 s, which means more active power is supplied to grid as amount of active load demand is reduced due to phase removal of nonlinear load. The grid reactive power output (Q_G) is zero as the VSC supplies the reactive power requirements of the load. There is a decrease in ψ_{lp} due to load phase removal, while ψ_{pv} remains constant as SPV power (P_{PV}) is unchanged due to constant solar insolation in this case, resulting in more negative value of ψ_{sp}. The VSC-DC-link voltage (V_{DC}) and magnitude of point of common coupling voltage (V_t) are still well maintained at 700 V and 415 V, respectively. The total harmonic distortion value for the grid voltage and load current is also presented. The % THD in grid current is found to be 0.91% which is well in agreement with the 5% suggested by the IEEE-519 standard.

4.3 Dynamic Behaviour Under Variable Solar Irradiance

Figure 5 illustrates the dynamic behaviour of the system in case of simulated drop in irradiance to 600 W/m^2 from 1000 W/m^2 at 0.4 s. As the solar irradiance decreases, the extracted SPV power from the SPV (P_{PV}) is reduced; as such the active power output of the VSC is reduced. The output current of the SPV array (I_{PV}) and the grid currents (i_g) also decrease. The active power output of the grid (P_G) continues to be negative but increases to a value less negative than earlier as a reduced amount of power is available to be supplied back to the grid. The maximum power point operation of the

controller is appropriate with the change in the solar irradiance along with VSC-DC-link voltage (V_{DC}) which is well sustained to 700 V. The reactive output power of the grid (Q_G) is again zero. Three-phase PCC voltage (v_g) waveform and three-phase grid current (i_g) waveform remain sinusoidal. The load current (i_{La}) waveform and the VSC output current (i_{inv}) waveform for phase 'A' are also shown. The phase angle is 180 degree between each phase voltage and current of grid indicating grid's unity power factor operation. The grid phase current decreases after the change in irradiance, but the grid phase voltage remains the same. The % THD in grid current found to be 0.60% which is well in agreement with the 5% suggested by the IEEE-519 standard.

Figure 6 illustrates the dynamic behaviour of the system for a simulated drop in solar irradiance from 600 W/m^2 to zero at 0.6 s. As the SPV insolation is interrupted, hence, the SPV power drops to zero. The active power of VSC is now zero, and hence, it only supplies the reactive demand of the load. The active power output of the grid (P_G) now becomes positive which means that the active power demand of load is now supplied by the grid. This is shown in waveform of grid current (i_g) which illustrates the phase reversal of the grid current at zero crossing. The VSC-DC-link voltage (V_{DC}) is still well maintained at 700 V. The reactive power output of the grid (Q_G) is again zero. The phase grid voltage (v_g) waveform and phase grid current (i_g) waveform remain sinusoidal. The load current (i_{La}) waveform and the VSC output current (i_{inv}) waveform for phase 'A' are also shown. The voltage and current of each phase of grid are now in-phase and hence indicate grid's unity power factor operation. The % THD in grid current is found to be 0.58% which is well in agreement with the 5% suggested by the IEEE-519 standard.

4.4 Comparison of RA-IHSF Against Traditional Controls

The proposed RA-IHSF-based control technique is compared with traditional techniques by developing and simulating the Simulink models of conventional LMF and LMS control approach. In dynamic disturbances, oscillations in the active load weight component (ψ_{lp}) by the proposed RA-IHSF technique are less than LMS and comparable to LMF technique, while convergence speed of weight computation is more than LMF and comparable to LMS technique as illustrated in Fig. 7a. The proposed RA-IHSF control technique mitigates grid current harmonics more as compared to traditional ones as illustrated in terms of per cent THD in Fig. 7b, c and d. All these comparisons are summarized in Table 2.
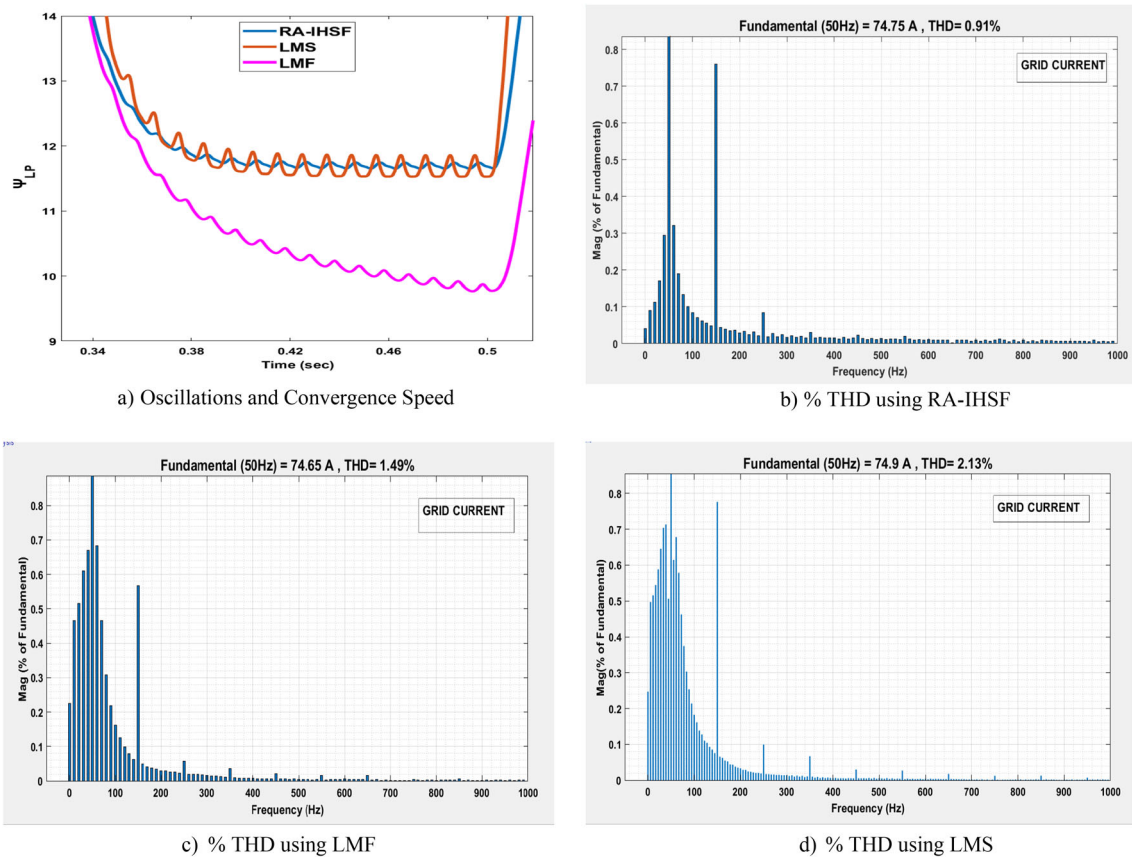
a) Oscillations and Convergence Speed

b) % THD using RA-IHSF

c) % THD using LMF

d) % THD using LMS

Fig. 7 Comparison of RA-IHSF with traditional techniques

Table 2 Comparison of RA-IHSF with traditional techniques

Control technique	THD level (%)	Convergence speed	Oscillations
RA-IHSF	0.91	Fast	Low
LMF	1.49	Slow	Low
LMS	2.13	Fast	High

5 Conclusion

The configuration of the grid integrated SPV system with proposed control algorithm is developed and simulated in Simulink environment of MATLAB. The proposed robust adaptive inverse hyperbolic sine function (RA-IHSF)-based control is employed to control the operation of VSC by altering the switching patterns of pulses. Thus, the proposed control approach provides the interfacing of SPV with the grid while maintaining grid current sinusoidal and balanced in dynamic disturbances such as load unbalancing and varying solar insolation. The proposed scheme provides load balancing and reactive power demand and mitigates harmonic content of grid current along with PFC. Maintaining

THD values as low as on a system can further assure improved equipment performance and a longer equipment life. Also, reduction in oscillations and better convergence speed are shown in weight computation by implementing RA-IHSF technique. Thus, a much better performance is demonstrated for the developed system when employed with proposed RA-IHSF technique in place of traditional techniques. In the booming era of electric vehicles (EVs), the proposed control approach of VSC can be implemented for operation of charging stations for EVs powered with grid integrated SPV systems.

References

1. Steffel, S.J.; Caroselli, P.R.; Dinkel, A.M.; Liu, J.Q.; Sackey, R.N.; Vadhar, N.R.: Integrating solar generation on the electric distribution grid. IEEE Trans .Smart Grid **3**(2), 878–886 (2012). https://doi.org/10.1109/TSG.2012.2191985

2. Kumar, A.; Kumar, P.: Power quality improvement for grid-connected PV system based on distribution static compensator with fuzzy logic controller and UVT/ADALINE-based least mean square controller. J. Mod. Power Syst. Clean Energy **9**(6), 1289–1299 (2021). https://doi.org/10.35833/MPCE.2021.000285

3. Hamrouni, N.; Jraidi, M.; Dhouib, A.; Cherif, A.: Design of a command scheme for grid connected PV systems using classical

controllers. Electric Power Syst. Res. **143**, 503–512 (2017). https://doi.org/10.1016/j.epsr.2016.10.064

4. Rana, S.A., Jamil, M., Khan, M.A., Aalam, M.N.: Zero attracting mixed norm LMS (ZA-MNLMS) control for two-stage power conversion of grid interfaced solar PV system, In: 2022 IEEE Delhi Section Conference (DELCON), Feb. 2022, pp. 1–5. https://doi.org/10.1109/DELCON54057.2022.9752839

5. Yao, E.; Samadi, P.; Wong, V.W.S.; Schober, R.: Residential demand side management under high penetration of rooftop photovoltaic units. IEEE Trans. Smart Grid **7**(3), 1597–1608 (2016). https://doi.org/10.1109/TSG.2015.2472523

6. Barnes, A.K.; Balda, J.C., Stewart, C.M.: Selection of converter topologies for distributed energy resources, In: 2012 Twenty-Seventh Annual IEEE Applied Power Electronics Conference and Exposition (APEC), Feb. 2012, pp. 1418–1423. doi: https://doi.org/10.1109/APEC.2012.6166006

7. Nazir, F.U.; Kumar, N.; Pal, B.C.; Singh, B.; Panigrahi, B.K.: Enhanced SOGI controller for weak grid integrated solar PV system. IEEE Trans. Energy Convers. **35**(3), 1208–1217 (2020). https://doi.org/10.1109/TEC.2020.2990866

8. Naqvi, S.B.Q.; Kumar, S.; Singh, B.: Three-phase four-wire PV system for grid interconnection at weak grid conditions. IEEE Trans. Ind. Appl. **56**(6), 7077–7087 (2020). https://doi.org/10.1109/TIA.2020.3020931

9. Kihal, A.; Krim, F.; Talbi, B.; Laib, A.; Sahli, A.: A robust control of two-stage grid-tied PV systems employing integral sliding mode theory. Energies (Basel) **11**(10), 2791 (2018). https://doi.org/10.3390/en11102791

10. Qaiser Naqvi, S.B., Singh, B.: A single-stage three-phase four-wire grid integrated multifunctional PV system with improved performance at challenging grid scenarios," In: Conference Record - IAS Annual Meeting (IEEE Industry Applications Society), 2021, vol. 2021-October. https://doi.org/10.1109/IAS48185.2021.9677328

11. Reddy, D., Ramasamy, S.: A fuzzy logic MPPT controller based three phase grid-tied solar PV system with improved CPI voltage," In: 2017 Innovations in Power and Advanced Computing Technologies (i-PACT), Apr. 2017, vol. 2017-January, pp. 1–6. https://doi.org/10.1109/IPACT.2017.8244953

12. Badoni, M.; Singh, A.; Singh, V.P.; Tripathi, R.N.: Grid interfaced solar photovoltaic system using ZA-LMS based control algorithm. Electric Power Syst. Res. **160**, 261–272 (2018). https://doi.org/10.1016/j.epsr.2018.03.001

13. Agarwal, R.K.; Hussain, I.; Singh, B.: LMF-based control algorithm for single stage three-phase grid integrated solar PV system. IEEE Trans. Sustain. Energy **7**(4), 1379–1287 (2016). https://doi.org/10.1109/TSTE.2016.2553181

14. Bakar Siddique, M.A.; Asad, A.; Asif, R.M.; Rehman, A.U.; Sadiq, M.T.; Ullah, I.: Implementation of incremental conductance MPPT algorithm with integral regulator by using boost converter in grid-connected PV array. IETE J. Res. (2021). https://doi.org/10.1080/03772063.2021.1920481

15. Ram, J.P.; Babu, T.S.; Rajasekar, N.: A comprehensive review on solar PV maximum power point tracking techniques. Renew. Sustain. Energy Rev. **67**, 826–847 (2017). https://doi.org/10.1016/j.rser.2016.09.076

16. Xiao, W., Dunford, W.G.: A modified adaptive hill climbing MPPT method for photovoltaic power systems, In: 2004 IEEE 35th Annual Power Electronics Specialists Conference (IEEE Cat. No.04CH37551), 2004, pp. 1957–1963 Vol.3, https://doi.org/10.1109/PESC.2004.1355417

17. Enrique, J.M.; Andújar, J.M.; Bohórquez, M.A.: A reliable, fast and low cost maximum power point tracker for photovoltaic applications. Sol. Energy **84**(1), 79–89 (2010). https://doi.org/10.1016/j.solener.2009.10.011

18. Gounden, N.A.; Ann Peter, S.; Nallandula, H.; Krithiga, S.: Fuzzy logic controller with MPPT using line-commutated inverter for three-phase grid-connected photovoltaic systems. Renew. Energy **34**(3), 909–915 (2009). https://doi.org/10.1016/j.renene.2008.05.039

19. Farhat, M.; Barambones, O.; Sbita, L.: Efficiency optimization of a DSP-based standalone PV system using a stable single input fuzzy logic controller. Renew. Sustain. Energy Rev. **49**, 907–920 (2015). https://doi.org/10.1016/j.rser.2015.04.123

20. Anh, H.P.H.: Implementation of supervisory controller for solar PV microgrid system using adaptive neural model. Int. J. Electr. Power Energy Syst. **63**, 1023–1029 (2014). https://doi.org/10.1016/j.ijepes.2014.06.068

21. Liu, Y.-H.; Huang, S.-C.; Huang, J.-W.; Liang, W.-C.: A particle swarm optimization-based maximum power point tracking algorithm for PV systems operating under partially shaded conditions. IEEE Trans. Energy Convers. **27**(4), 1027–1035 (2012). https://doi.org/10.1109/TEC.2012.2219533

22. Saad, N.H.; El-Sattar, A.A.; Mansour, A.E.A.M.: Improved particle swarm optimization for photovoltaic system connected to the grid with low voltage ride through capability. Renew. Energy **85**, 181–194 (2016). https://doi.org/10.1016/j.renene.2015.06.029

23. Singh, B., Solanki, J.: A comparative study of control algorithms for DSTATCOM for load compensation," In: 2006 IEEE International Conference on Industrial Technology, 2006, pp. 1492–1497. https://doi.org/10.1109/ICIT.2006.372413

24. Singh, B.; Chandra, A.; Al-Haddad, K.: Power Quality Problems and Mitigation Techniques. Wiley, Chichester (2015)

25. Zaveri, N., Mehta, A., Chudasama, A.: Performance analysis of various SRF methods in three phase shunt active filters, In: 2009 International Conference on Industrial and Information Systems (ICIIS), Dec. 2009, pp. 442–447. https://doi.org/10.1109/ICIINFS.2009.5429819

26. Seema, A.K.; Singh, B., Jain, R.: Modified NVSSLMS based control for single stage 3P3W grid-interfaced PV system," In: 2020 IEEE International Conference on Power Electronics, Smart Grid and Renewable Energy (PESGRE2020), Jan. 2020, pp. 1–6. https://doi.org/10.1109/PESGRE45664.2020.9070661

27. Shah, P.; Singh, B.: Adaptive observer based control for rooftop solar PV system. IEEE Trans. Power Electron. **35**(9), 9402–9415 (2020). https://doi.org/10.1109/TPEL.2019.2898038

28. George, S.A., Chacko, F. M.: Comparison of different control methods for integrated system of MPPT powered PV module and STATCOM," In: Proceedings - 2013 International Conference on Renewable Energy and Sustainable Energy, ICRESE 2013, 2014. https://doi.org/10.1109/ICRESE.2013.6927816

29. Tripathi, R.N., Singh, A.: SRF theory based grid interconnected Solar Photovoltaic (SPV) system with improved power quality, In: Proceedings - 2013 International Conference on Emerging Trends in Communication, Control, Signal Processing and Computing Applications, IEEE-C2SPCA 2013, 2013. https://doi.org/10.1109/C2SPCA.2013.6749390

30. Kesler, M.; Ozdemir, E.: Synchronous-reference-frame-based control method for UPQC under unbalanced and distorted load conditions. IEEE Trans. Ind. Electron. **58**(9), 3967–3975 (2011). https://doi.org/10.1109/TIE.2010.2100330

31. Singh, A.K.; Hussain, I.; Singh, B.: Double-stage three-phase grid-integrated solar PV system with fast zero attracting normalized least mean fourth based adaptive control. IEEE Trans. Ind. Electron. **65**(5), 3921–3931 (2018). https://doi.org/10.1109/TIE.2017.2758750

32. Kewat, S.; Singh, B.: Improved reweighted zero-attracting quaternion-valued LMS algorithm for islanded distributed generation system at IM Load. IEEE Trans. Ind. Electron. **67**(5), 3705–3716 (2020). https://doi.org/10.1109/TIE.2019.2916301

33. Singh, S.; Kewat, S.; Singh, B.; Panigrahi, B.K.: Enhanced momentum LMS-based control technique for grid-tied solar system. IET

Power Electron. **13**(13), 2767–2774 (2020). https://doi.org/10.1049/iet-pel.2019.1126

34. Singh, B.; Dube, S.K.; Arya, S.R.: Hyperbolic tangent function-based least mean-square control algorithm for distribution static compensator. IET Gener. Transm. Distrib. **8**(12), 2102–2113 (2014). https://doi.org/10.1049/iet-gtd.2014.0172

35. Kumar, A.; Kewat, S.; Singh, B.; Jain, R.: CC-ROGI-FLL based control for grid-tied photovoltaic system at abnormal grid conditions. IET Gener. Trans. Distrib. **14**(17), 3400–3411 (2020). https://doi.org/10.1049/iet-gtd.2019.0765

36. Kumar, V.N.; Pea, N.B.; Kiranmayi, R.; Siano, P.; Panda, G.: Improved power quality in a solar PV plant integrated utility grid by employing a novel adaptive current regulator. IEEE Syst. J **14**(3), 4308–4319 (2020). https://doi.org/10.1109/JSYST.2019.2958819

37. Sahoo, S.K.; Kumar, S.; Singh, B.: VSSMLMS-based control of multifunctional PV-DSTATCOM system in the distribution network. IET Gener. Transm. Distrib. **14**(11), 2100–2110 (2020). https://doi.org/10.1049/iet-gtd.2019.0889

38. Walach, E.; Widrow, B.: The least mean fourth (LMF) adaptive algorithm and its family. IEEE Trans. Inf. Theor. **30**(2), 275–283 (1984). https://doi.org/10.1109/TIT.1984.1056886

39. Devi, S.C.; Singh, B.; Devassy, S.: Modified generalised integrator based control strategy for solar PV fed UPQC enabling power quality improvement. IET Gener. Trans. Distrib. **14**(16), 3127–3138 (2020). https://doi.org/10.1049/iet-gtd.2019.1939

40. Guan, S.; Cheng, Q.; Zhao, Y.; Biswal, B.: Robust adaptive filtering algorithms based on (inverse)hyperbolic sine function. PLoS ONE **16**(10), e258155 (2021). https://doi.org/10.1371/journal.pone.0258155